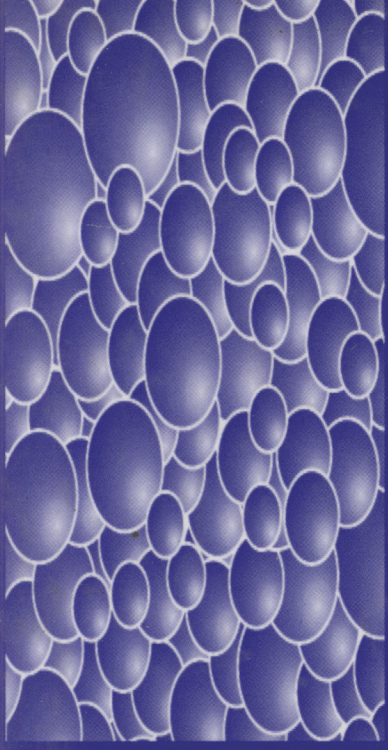

RS•C

Granular Materials

FUNDAMENTALS AND APPLICATIONS

edited by S. JOSEPH ANTONY, W. HOYLE and YULONG DING

Granular Materials
Fundamentals and Applications

Edited by

S. Joseph Antony
School of Process, Environmental and Materials Engineering, University of Leeds, UK

W. Hoyle
Consultant, Stockport, UK

Yulong Ding
School of Process, Environmental and Materials Engineering, University of Leeds, UK

RS•C
advancing the chemical sciences

ISBN 0–85404–586–4

A catalogue record for this book is available from the British Library

Published by The Royal Society of Chemistry,
Thomas Graham House, Science Park, Milton Road,
Cambridge CB4 0WF, UK

Registered Charity Number 207890

For further information see our web site at www.rsc.org

Typeset by RefineCatch Limited, Bungay, Suffolk, UK
Printed by Athenaeum Press Ltd, Gateshead, Tyne and Wear, UK

Preface

Granular materials are an important part of several engineering applications of technological importance. The industries that handle granular materials include food preparation, pharmaceutical, consumer products, agricultural products, metal powders, mechanical, geotechnical, chemical, nuclear and green industries. In addition, high rates of innovation in these industries means that there is a continuous need for achieving excellence in predicting the fundamental behaviour of granular materials under different working environments. Analysis of physical systems involving granular materials requires clear understanding of their behaviour not only at the single particle level, but should also consider the solutions of multi-physics problem involving multi-scale phenomena from molecular to macroscopic scale.

In this book, we present the recent advances made in theoretical, computational and experimental approaches in understanding the often mysterious behaviour of granular materials, including industrial applications. The approaches presented here are complementary and provide a collective understanding of the behaviour of granular materials. All the chapters, with the right blend of basics and advances, are presented by leading experts from around the world, who have many years experience in their fields.

Chapters one to seven deal with the recent advances made on the fundamental concepts of granular materials. The first chapter presents the quasi-static deformation characteristics of granular materials at both small and large strains. The particles have been considered as a discrete system in the analysis. The second chapter focuses on the effects of mechanical periodic excitation on a granular medium, dealing with several fundamental issues. The third chapter presents the advances made on the constitutive modelling of granular materials using a continuum approach. The behaviour of particle interactions at elevated temperatures, including adhesion forces and sintering phenomena is presented in chapter four. In this chapter a novel off-line technique has been presented for the determination of actual high temperature interactions. The next chapter examines the critical state behaviour of granular materials under several initial conditions using three-dimensional discrete element modelling. The sixth chapter presents the key features of granular plasticity, providing an insight into the macroscopic trends from the lowest level description of granular microstructure.

The concluding chapter of the first section on the fundamental concepts describes the advances made on the use of Atomic Forces Microscopy (AFM) as a measurement tool to investigate particle interactions, and in particular those in the presence of polymers.

Chapters eight to thirteen present the recent advances made in experimental measurement techniques, and several industrial applications dealing with granular materials. The first of these chapters focuses on the measurement of granular forces in dry systems using AFM. Aspects covered include humid air and conditions under which the particle surfaces may be modified by liquid films or coatings, since such conditions are of great technological importance.

A weakness in the ability to develop sophisticated granular models is the lack of suitable experimental validation methods. Ideally, these methods should be in-situ and not perturb the process modelled in any way. The ninth chapter presents several examples of such methods that can be applied to dry and wet particulate systems. The tenth chapter reviews the fluidisation characteristics of fine particles together with aids in fluidising fine powders. Effects of temperature on fine powder fluidisation are also covered. This chapter ends with the discussion of selected applications and potential applications. The eleventh chapter introduces and reviews various modelling approaches at different length scales for the prediction of granulation under high shear conditions.

Rotary kilns are widely used in the processing of granular solids in the chemical and metallurgical industries. Chapter twelve describes work done at Cambridge University on the dynamics of particle motion in rotary kilns, using cold laboratory scale equipment. The final chapter presents both the theoretical and experimental aspects of granular motion in the transverse plane of rotating drums. Experimental results presented in this chapter were obtained exclusively by using the Positron Emission Particle Tracking (PEPT) technique.

We hope that this book will serve as an excellent reference for scientists, engineers and students working across a wide spectrum of engineering disciplines dealing with granular materials.

We are very grateful to all the contributors for giving so generously of their valuable time and making it possible to produce this book. The support provided by the Royal Society of Chemistry, Cambridge, UK in publishing this book is gratefully acknowledged by the editors.

S. Joseph Antony
Bill Hoyle
Yulong Ding

Contents

Fundamentals

CHAPTER 1

Rates of Stress in Dense Unbonded Frictional Materials During Slow Loading

MATTHEW R. KUHN

University of Portland, 5000 N. Willamette Blvd, Portland, OR 97203 U.S.A.
Email: kuhn@up.edu

1 Introduction

This chapter concerns the transmission and evolution of stress within granular materials during slow, quasi-static deformation. Stress is a continuum concept, and its application to assemblies of discrete grains requires an appreciation of the marked nonuniformity of stress when measured at the scale of individual grains or grain clusters. As an example, numerous experiments and simulations have demonstrated that externally applied forces are borne disproportionately by certain grains that are arranged in irregular and ever-changing networks of *force chains*.[1,2,3] Although much attention has recently been given to the transmission of force at low strains, the current work focuses on the transmission of stress within granular materials at both small and large strains.

When a densely packed assembly of unbonded particles is loaded in either triaxial compression or shear, the behaviour at small strains is nearly elastic, and the volume is slightly reduced by the initial loading (an initial Poisson ratio less than 0.5, Figure 1). Plastic deformation ensues at moderate strains, at which an initially dense material becomes dilatant, and this trend of increasing volume continues during strain hardening, at the peak strength, and during strain softening. At very large strains, the material reaches a steady condition of flow, referred to as the "critical state" in geotechnical engineering practice, in which the material flows at a constant, albeit expanded, volume while sustaining a constant shearing or compressive effort.[4] Besides studying behaviour at the initial and peak states, we will also consider experimental results at this steady state condition and the manner in which the inter-granular forces are distributed and changed during steady state flow. These conditions are investigated with

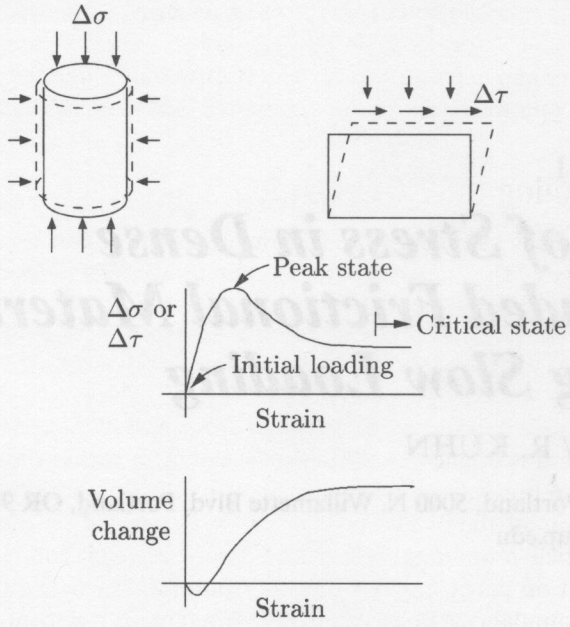

Figure 1 *Typical behaviour of a dense granular material during shearing or unconfined compression to large strains*

numerical simulations of an idealized assembly of circular disks. We will explore mechanisms that underlie the changing stress rate into various constituents and then study their relative influences during simulated loading.

Notation

In this chapter, vectors and tensors are represented in both indexed and unindexed forms with the use of upper and lower case glyphs: $\mathbf{A}$ or A_{ij} for tensors, and $\mathbf{a}$ or a_i for vectors. Inner products are computed as

$$\mathbf{a} \cdot \mathbf{b} = a_i b_i, \; \mathbf{A} \cdot \mathbf{B} = A_{ij} B_{ij}, \tag{1}$$

and tensors are often represented as the dyadic products of vectors:

$$\mathbf{a} \otimes \mathbf{b} = a_i b_j. \tag{2}$$

A juxtaposed tensor and vector will represent the conventional product

$$\mathbf{A}\mathbf{b} = A_{ij} b_j. \tag{3}$$

No contraction is implied with superscripts (e.g., $\mathbf{a}^c\mathbf{b}^c$). The *trace* of a tensor is defined as

$$\text{trace}\,(\mathbf{A}) = A_{11} + A_{22} + A_{33}. \tag{4}$$

Tensile stresses and extension strains are positive, although the pressure p will be positive for compressive conditions.

2 Partitioning the Stress Rate

The average Cauchy stress $\overline{\boldsymbol{\sigma}}$ within a granular assembly can be computed as a weighted average of the contact forces between grains:[5,6]

$$\overline{\boldsymbol{\sigma}} = \frac{1}{V}\sum_{c\in\mathcal{M}} \mathbf{f}^c \otimes \mathbf{l}^c, \tag{5}$$

where summation is applied to the set of $\mathcal{M}$ contacts within the assembly, and each contact c represents an ordered pair of contacting particles p and q, $c = (p, q)$. The sum is of the dyadic products $\mathbf{f}^c \otimes \mathbf{l}^c$, where $\mathbf{f}^c$ is the contact force exerted by particle q upon particle p, and *branch vector* $\mathbf{l}^c$ connects a reference (material) point on particle p to a reference point on particle q (Figure 2). For the numerical simulations in this study, these reference points are placed at the centres of circular disks. The current volume (area) of the three-dimensional (two-dimensional) region is represented by V. Equation 5 applies, of course, only under ideal conditions. The absence of kinetic terms limits Equation 5 to slow, quasi-static deformation, and the lack of body force terms implies a zero-gravity condition.[7] Equation 5 also avoids the complexities that are associated with peripheral particles in a finite region and with contacts that can transmit couples between particle pairs.[8] Although these complexities can be difficult to evaluate in physical experiments, they can be circumvented altogether in numerical simulations that exclude both gravity forces and contact moments, and in which the boundaries are periodic.

The formulation (5) for average stress has been employed in a number of ways.

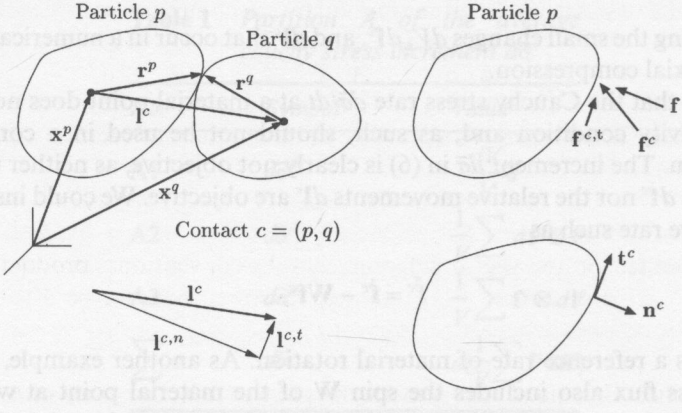

Figure 2 *Position and force for a pair of contacting particles*

Its use in numerical simulations allows the direct calculation of stress from the inter-particle contact forces, but without the supplemental operation of identifying boundary particles and computing the external forces on those particles, an advantage that is particularly appropriate when the boundaries are periodic. Equation 5 has also been the starting point for estimating a macro-scale stiffness from the micro-scale behaviour at particle contacts, and modest successes have been reported at small strains.[9–11] The equation has also led to important insights into the nature of stiffness and strength in granular materials. These insights have been primarily gained by partitioning the average stress $\overline{\boldsymbol{\sigma}}$ into various contributions that arise from the distributions and directions of the contact forces $\mathbf{f}^c$. Several studies have partitioned the stress into two contributions: one from the normal components of the contact forces, and the other from the tangential components.[12–15] These studies have shown that the average stress is borne largely by the normal forces, and although the macroscopic strength is greatly reduced when contacts are rendered frictionless, the contribution of the tangential forces to $\overline{\boldsymbol{\sigma}}$ is small, even when the contacts are frictional. Cundall[12] partitioned the average deviatoric stress into contributions from the tangential forces, from the anisotropic distribution of contact orientations, and from the anisotropic distribution of normal contact forces. The average deviatoric stress was shown to be supported primarily by the relative prevalence and intensity of the normal contact forces that are roughly aligned with the direction of the major principal compressive stress.

The current work concerns the manner in which the average stress $\overline{\boldsymbol{\sigma}}$ *changes during loading*, and, in this regard, we consider a stress rate $d\overline{\boldsymbol{\sigma}}/dt$ derived from Equation 5a. We will partition the stress in three different ways so that internal processes can be investigated within a model granular material. The separate participation of V, $\mathbf{f}^c$, and $\mathbf{l}^c$ in the stress rate will be investigated with the differential form

$$d\overline{\boldsymbol{\sigma}} = -\frac{dV}{V}\overline{\boldsymbol{\sigma}} + \sum_{c\in\mathcal{M}} d\mathbf{f}^c \otimes \mathbf{l}^c + \sum_{c\in\mathcal{M}} \mathbf{f}^c \otimes d\mathbf{l}^c, \tag{6}$$

by measuring the small changes dV, $d\mathbf{f}^c$, and $d\mathbf{l}^c$ that occur in a numerical simulation of biaxial compression.

We note that the Cauchy stress rate $d\overline{\boldsymbol{\sigma}}/dt$ at a material point does not satisfy the objectivity condition and, as such, should not be used in a constitutive formulation. The increment $d\overline{\boldsymbol{\sigma}}$ in (6) is clearly not objective, as neither the force increments $d\mathbf{f}^c$ nor the relative movements $d\mathbf{l}^c$ are objective. We could instead use an objective rate such as

$$\mathring{\mathbf{f}}^c = \dot{\mathbf{f}}^c - \mathbf{W}\mathbf{f}^c, \tag{7}$$

where $\mathbf{W}$ is a reference rate of material rotation. As another example, the Jaumann stress flux also includes the spin $\mathbf{W}$ of the material point at which the stress rate is being measured. The spin $\mathbf{W}$ could, however, be taken from *any*

other material point, however distant, or as a weighting of the spins at numerous distant points, provided that the weights sum to one. By including distant spins in the computation of an objective rate, we must obviously forfeit the usual assumption of local action. In the current context, however, we compute an objective *average stress rate*, which is local only to an entire material region, and the principal of local action at a material point has no meaning in this setting. In the current simulations, we use the average spin $\overline{\mathbf{W}}$ among all particles in an assembly to compute an objective stress rate. Because this average spin is nearly zero for the conditions of biaxial compression that are being considered, the spin $\overline{\mathbf{W}}$ is entirely neglected in the stress increment of equation 6.

The expression for $d\bar{\sigma}$ in equation 6 does not explicitly account for changes in the set $\mathcal{M}$ of particle contacts, even though few contacts are likely to be persistent throughout a period of sustained deformation. We note, however, that the set $\mathcal{M}$ could also be the set of *all particle pairs*, not just those that are in contact (in this case, only the subset of contacting pairs would contribute non-zero forces $\mathbf{f}^c$). The numerical simulations in this study use a time-stepping procedure, and we account for the contacts that are newly formed (or disengaged) within the span of each time step, and we also account for the fractions of a time step over which such contacts are engaged.

2.1 Partition A of the Stress Increment $d\bar{\sigma}$

Form (6) will be used to explore the evolution of stress in granular materials, and it will serve as the basis for even finer partitions of the stress rate. The terms in equation 6 will be represented as

$$d\bar{\sigma} = d\bar{\sigma}^{dv} + d\bar{\sigma}^{df} + d\bar{\sigma}^{d\ell}, \tag{8}$$

and are also listed in Table 1. At low strain, we would expect the second term, $d\bar{\sigma}^{df}$, to be dominant. Changes in the contact forces $d\mathbf{f}^c$ depend upon changes in the contact indentations, but even large changes in indentation will produce only

Table 1 *Partition A of the average cauchy stress increment* $d\bar{\sigma}$

No.	*Symbol*	*Value*[a]
A1	$d\bar{\sigma}^{dv}$	$-\frac{dV}{V}\bar{\sigma}$
A2	$d\bar{\sigma}^{df}$	$\frac{1}{V}\sum d\mathbf{f}^c \otimes \mathbf{l}^c$
A3	$d\bar{\sigma}^{d\ell}$	$\frac{1}{V}\sum \mathbf{f}^c \otimes d\mathbf{l}^c$
$\sum =$	$d\bar{\sigma}$	$d(\frac{1}{V}\sum \mathbf{f}^c \otimes \mathbf{l}^c)$

[a] Sums Σ are for the set of particle contacts $c \in \mathcal{M}$.

small increments $d\mathbf{l}^c$ in the branch vectors between the centres of contacting particles (Figure 2). (In the current simulations, the average contact indentation is only about 5×10^{-4} of the average particle size.) The volume contribution $d\bar{\boldsymbol{\sigma}}^{dv}$ will also be negligible for dense packings at small strains, since the bulk modulus will be much larger than the stress.

A primary concern of the current study is the behaviour at large strains, where the material reaches a critical, steady state condition of zero stress change and zero volume change. For this situation, both $d\bar{\boldsymbol{\sigma}}$ and $d\bar{\boldsymbol{\sigma}}^{dv}$ in equation 8 will be zero, and the two contributions $d\bar{\boldsymbol{\sigma}}^{df}$ and $d\bar{\boldsymbol{\sigma}}^{d\ell}$ will be of comparable magnitude, although, as will be seen, neither term can be zero. We will investigate both contributions to the stress rate $d\bar{\boldsymbol{\sigma}}$ during critical state deformation. These contributions, $d\bar{\boldsymbol{\sigma}}^{df}$ and $d\bar{\boldsymbol{\sigma}}^{d\ell}$, can be more fully understood by two further decompositions of these stress increments, as in the remaining Partitions B and C.

2.2 Partition B of the Stress Increments $d\bar{\boldsymbol{\sigma}}^{df}$ and $d\bar{\boldsymbol{\sigma}}^{d\ell}$

2.2.1 Partition B of Stress Increment $d\bar{\boldsymbol{\sigma}}^{df}$

In this section, we derive four contributions to the changes in the contact forces $\{d\mathbf{f}^c: c \in \mathcal{M}\}$ and to their cumulative effect on the stress increment, $d\bar{\boldsymbol{\sigma}}^{df}$. The stress increment $d\bar{\boldsymbol{\sigma}}^{df}$, the second term in Partition A (Equations 6 and 8), can be expressed as the sum of these four contributions:

1. $d\bar{\boldsymbol{\sigma}}^{df;\,\text{unif.-elast.}}$: This increment is the change in stress that would be produced by the force increments $d\mathbf{f}^c$ if the particles did not rotate and if the motions of their centres conformed to the mean deformation of the entire assembly. With this contribution, the contact mechanism is also assumed to be elastic. The particles will, of course, rotate; their movements will not conform to a uniform, affine deformation condition; and the contact interactions will likely produce frictional slipping and plastic deformation. By conducting realistic numerical simulations, we can determine the actual movements, rotations, and contact interactions of a model assembly. This data will allow the calculation of the following three corrections to $d\bar{\boldsymbol{\sigma}}^{df;\,\text{unif.-elast.}}$.
2. $d\bar{\boldsymbol{\sigma}}^{df;\,\text{fluct.-elast.}}$: This increment is the change in stress due solely to fluctuations of the particle motions from a uniform deformation field, but with elastic contacts and no particle rotations.
3. $d\bar{\boldsymbol{\sigma}}^{df;\,\text{rotate-elast.}}$: This increment is the change in stress due solely to the measured particle rotations, but neglecting the effects of any inelastic contact behaviour.
4. $d\bar{\boldsymbol{\sigma}}^{df;\,\text{slide}}$: This increment is the change in stress that can be attributed to inelastic contact behaviour.

Taken together, the stress increment $d\bar{\boldsymbol{\sigma}}^{df}$ in equation 8 is the sum of the four contributions,

$$d\bar{\boldsymbol{\sigma}}^{df} = d\bar{\boldsymbol{\sigma}}^{df;\,\text{unif.-elast.}} + d\bar{\boldsymbol{\sigma}}^{df;\,\text{fluct.-elast.}} + d\bar{\boldsymbol{\sigma}}^{df;\,\text{rotate-elast.}} + d\bar{\boldsymbol{\sigma}}^{df;\,\text{slide}}, \tag{9}$$

and these contributions are detailed below.

The change in a contact force $d\mathbf{f}^c$ depends upon the relative movement $d\boldsymbol{v}^c$ of the particles p and q at the contact point c, with

$$d\boldsymbol{v}^c = d\mathbf{u}^q - d\mathbf{u}^p + d\boldsymbol{\Omega}^q\mathbf{r}^{c,q} - d\boldsymbol{\Omega}^p\mathbf{r}^{c,p}. \tag{10}$$

In this equation, movements $d\mathbf{u}^{(\cdot)}$ are the incremental particle translations, $d\boldsymbol{\Omega}^{(\cdot)}$ are the incremental particle rotation tensors, and $\mathbf{r}^{c,(\cdot)}$ are the vectors joining the centres of particles p and q with the contact point c (Figure 2). The particle translations $d\mathbf{u}^{(\cdot)}$ can be expressed as fluctuations $d\Delta^{(\cdot)}$ from the uniform, average deformation field, or

$$d\mathbf{u}^{(\cdot)} = \bar{\mathbf{L}}\mathbf{x}^{(\cdot)} + d\Delta^{(\cdot)}, \tag{11}$$

where $\bar{\mathbf{L}}$ is the average Eulerian velocity gradient (the sum of the average rate of deformation $\bar{\mathbf{D}}$ and the average assembly spin $\bar{\mathbf{W}}$), and $\mathbf{x}^{(\cdot)}$ is the particle position (Figure 2).

For non-linear or inelastic contacts, the force increment will depend upon the history of movements at a contact. With the simple spring-slider mechanism that is used in the current simulations, the increment $d\mathbf{f}^c$ can be written as

$$d\mathbf{f}^c = \mathbf{g}^c\,(d\boldsymbol{v}^c, \mathbf{f}^c), \tag{12}$$

where $\mathbf{f}^c$ is the current contact force. The force increment in equation 12 can be expressed as

$$d\mathbf{f}^c = \mathbf{g}^{c,\text{elastic}}\,(d\boldsymbol{v}^c, \mathbf{f}^c) + d\mathbf{f}^{c,\text{slide}}, \tag{13}$$

where the first term gives the change in force that would occur in the absence of inelastic contact deformation. The second term in equation 13 is an adjustment that accounts for any inelastic contact behaviour, such as that due to frictional slipping, contact crushing, or other plastic deformations. The simulations in this study employ a simple linear spring at the contact between two particles, and this spring is placed in series with a frictional slider. For this linear spring-slider mechanism, the elastic force increment in Equation 13 is simply

$$\mathbf{g}^{c,\text{elastic}}\,(d\boldsymbol{v}^c, \mathbf{f}^c) = \mathbf{K}^c d\boldsymbol{v}^c \tag{14}$$

$$\mathbf{K}^c = k^n\,\mathbf{n}^c \otimes \mathbf{n}^c + k^t\,(\boldsymbol{\delta} - \mathbf{n}^c \otimes \mathbf{n}^c), \tag{15}$$

where k^n and k^t are the normal and tangential spring stiffnesses, and δ is the Kronecker identity tensor.[16]

By gathering Equations 10, 11, and 14, the force increment $d\mathbf{f}^c$ in Equation 13 is

$$d\mathbf{f}^c = d\mathbf{f}^{c;\,\text{unif.-elast.}} + d\mathbf{f}^{c;\,\text{fluct.-elast.}} + d\mathbf{f}^{c;\,\text{rotate-elast.}} + d\mathbf{f}^{c;\,\text{slide}}, \tag{16}$$

with

$$d\mathbf{f}^{c;\,\text{unif.-elast.}} = \mathbf{K}^c(\overline{\mathbf{D}}dt)\mathbf{l}^c \tag{17}$$

$$d\mathbf{f}^{c;\,\text{fluct.-elast.}} = \mathbf{K}^c(d\boldsymbol{\Delta}^q - d\boldsymbol{\Delta}^p) \tag{18}$$

$$d\mathbf{f}^{c;\,\text{rotate.-elast.}} = \mathbf{K}^c\,[(d\boldsymbol{\Omega}^q - \overline{\mathbf{W}}dt)\mathbf{r}^q - (d\boldsymbol{\Omega}^p - \overline{\mathbf{W}}dt)\mathbf{r}^p] \tag{19}$$

$$d\mathbf{f}^{c;\,\text{slide}} = d\mathbf{f}^c - (d\mathbf{f}^{c;\,\text{unif.-elast.}} + d\mathbf{f}^{c;\,\text{fluct.-elast.}} + d\mathbf{f}^{c;\,\text{rotate-elast.}}). \tag{20}$$

The branch vector $\mathbf{l}^c$ in equation 17 is

$$\mathbf{l}^c = \mathbf{r}^p - \mathbf{r}^q = \mathbf{x}^q - \mathbf{x}^p \tag{21}$$

as shown in Figure 2. Because numerical simulations can track the particle motions and contact forces, each of the increments (17)–(20) can be computed for each contact within a granular assembly and then used to find the corresponding stress contributions in Equation 9:

$$d\overline{\boldsymbol{\sigma}}^{df;\,\text{unif.-elast.}} = \frac{1}{V}\sum_{c\in\mathcal{M}} \mathbf{K}^c(\overline{\mathbf{D}}\mathbf{l}^c dt)\otimes\mathbf{l}^c \tag{22}$$

$$d\overline{\boldsymbol{\sigma}}^{df;\,\text{fluct-elast.}} = \frac{1}{V}\sum_{c\in\mathcal{M}} \mathbf{K}^c(d\boldsymbol{\Delta}^q - d\boldsymbol{\Delta}^p)\otimes\mathbf{l}^c \tag{23}$$

$$d\overline{\boldsymbol{\sigma}}^{df;\,\text{rotate-elast.}} = \frac{1}{V}\sum_{c\in\mathcal{M}} \mathbf{K}^c[(d\boldsymbol{\Omega}^q - \mathbf{W}dt)\mathbf{r}^q) - (d\boldsymbol{\Omega}^p - \mathbf{W}dt)\mathbf{r}^p)]\otimes\mathbf{l}^c \tag{24}$$

$$d\overline{\boldsymbol{\sigma}}^{df;\,\text{slide}} = \frac{1}{V}\sum_{c\in\mathcal{M}} (d\mathbf{f}^c - d\mathbf{f}^{c,\,\text{elast.}})\otimes\mathbf{l}^c, \tag{25}$$

as is summarized in rows B1–B4 of Table 2. The presence of a linear contact stiffness tensor $\mathbf{K}^c$ in these equations applies only with linearly elastic contacts; but for non-linear contacts, stiffness $\mathbf{K}^c$ would be replaced by a non-linear function $\mathbf{g}^{c,\,\text{elastic}}$ as in Equation 14. If all contacts share the same linear stiffness $\mathbf{K}^c$, then the stress increment in Equation 22 is

$$d\overline{\boldsymbol{\sigma}}^{df;\,\text{unif.-elast.}} = \frac{1}{V}\mathbf{K}^c\overline{\mathbf{D}}\,dt\sum_{c\in\mathcal{M}} \mathbf{l}^c\otimes\mathbf{l}^c, \tag{26}$$

so that the stress increment $d\overline{\boldsymbol{\sigma}}^{df;\,\text{unif.-elast.}}$ depends only on the arrangement of particles (i.e., the assembly *fabric*) as expressed by the set of branch vectors $\{\mathbf{l}^c: c$